METRICA
METRology Institutional CAtalog

ISTITUTO NAZIONALE DI RICERCA METROLOGICA
Repository Istituzionale

Viscoelastic Characterization and Degradation Stability Investigation of Poly(butylene-adipate-co-terephthalate) - Calcium-Phosphate Glass Composites

Original
Viscoelastic Characterization and Degradation Stability Investigation of Poly(butylene-adipate-co-terephthalate) - Calcium-Phosphate Glass Composites / Togliatti, E., Milanese, D., Pugliese, D., Sciancalepore, C.. - In: JOURNAL OF POLYMERS AND THE ENVIRONMENT. - ISSN 1566-2543. - 30:9(2022), pp. 3914-3933. [10.1007/s10924-022-02479-1]

Availability:
This version is available at: 11696/77331 since:

Publisher:
Springer

Published
DOI:10.1007/s10924-022-02479-1

Terms of use:

This article is made available under terms and conditions as specified in the corresponding bibliographic description in the repository

Publisher copyright

(Article begins on next page)

14 October 2026

Journal of Polymers and the Environment (2022) 30:3914–3933
https://doi.org/10.1007/s10924-022-02479-1

ORIGINAL PAPER

Viscoelastic Characterization and Degradation Stability Investigation of Poly(butylene-adipate-co-terephthalate) – Calcium-Phosphate Glass Composites

Elena Togliatti[1,2] · Daniel Milanese[1,2] · Diego Pugliese[2,3] · Corrado Sciancalepore[1,2]

Accepted: 5 May 2022 / Published online: 6 June 2022
© The Author(s) 2022

Abstract
In this work new biodegradable composite materials based on poly(butylene-adipate-co-terephthalate) (PBAT) reinforced with water-soluble calcium-phosphate glass (CPG) microparticles at different filler concentration (0, 4, 10, 20 and 40 wt%) were characterized by dynamic-mechanical analysis (DMA), aging and fragmentation tests. DMA results showed increasing storage modulus (E') values with the filler content, without a significant modification of the glass transition temperature (T_g), translating in a reinforcing effect of the filler particles with good interphase adhesion. The creep compliance decreased with the increase of the CPG content, confirming a greater resistance of the composites to deformation under constant stress. The stability to weathering agents and the degree of fragmentation in laboratory-scale composting conditions were also tested, obtaining a higher sensitivity to degradation of the PBAT-based composites with the increase of CPG content. Overall, the addition of CPG particles in a PBAT matrix produced stiffer composites, with modulation of the properties based on the filler content, enhancing at the same time their degradation rate, making them a promising and more sustainable alternative to traditional polymers.

✉ Corrado Sciancalepore
corrado.sciancalepore@unipr.it

[1] Dipartimento di Ingegneria e Architettura, DIA, Università di Parma, Parco Area delle Scienze 181/A, 43124 Parma, Italy

[2] INSTM, Consorzio Interuniversitario Nazionale per la Scienza e Tecnologia dei Materiali, Via G. Giusti 9, 50121 Florence, Italy

[3] DISAT, Dipartimento di Scienza Applicata e Tecnologia, Politecnico di Torino, Corso Duca degli Abruzzi 24, 10129 Turin, Italy

Graphical Abstract

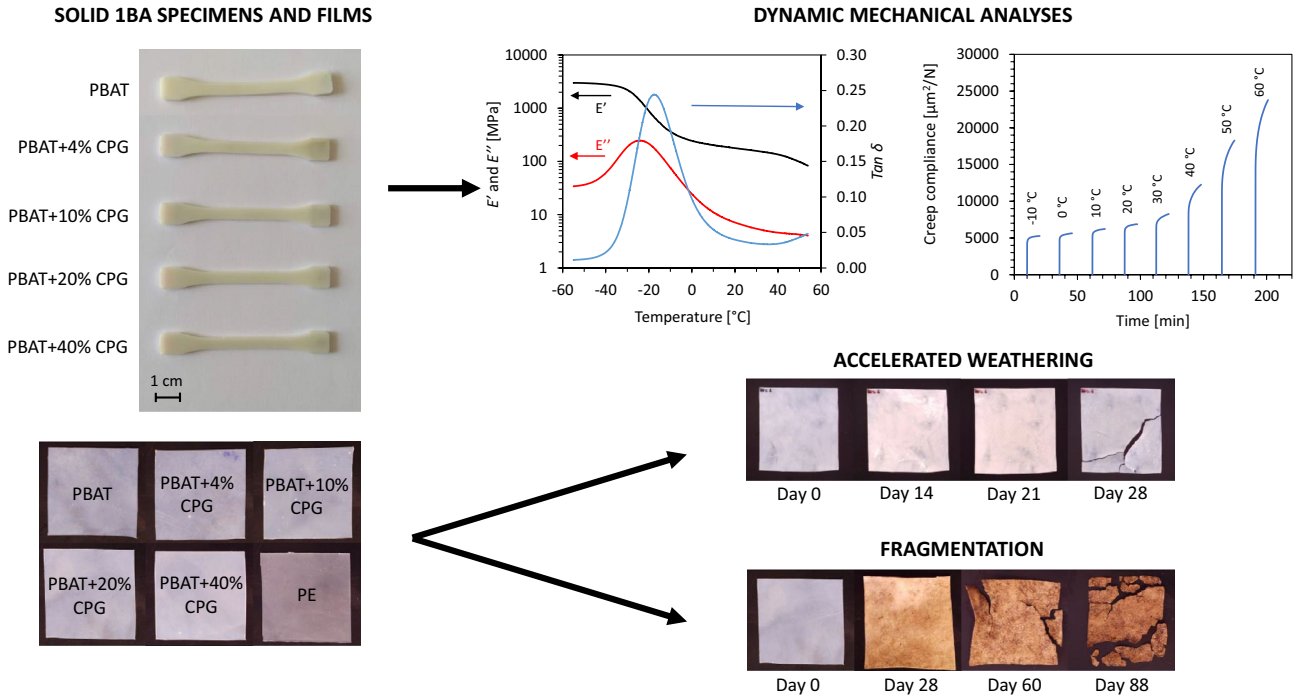

Keywords Biocomposites · Dynamic-mechanical properties · Weathering · Fragmentation

Introduction

Polymeric materials have been widely employed for decades in a large variety of fields [1] and, from many points of view, packaging is certainly the most important application, thanks to properties such as lightweight, good mechanical response, processability, in addition to interesting values of barrier properties to gases and water vapor [2].

In the last years, bioplastics have been taken into consideration and used for replacement of traditional ones because of the well-known environmental problems caused by improper handling of waste, leading to undesired phenomena like marine litter [3, 4] and soil pollution by microplastics [5].

Among the most diffused and studied biopolymers, poly(butylene-adipate-co-terephthalate) (PBAT) is a promising and increasingly diffused option, especially for packaging applications [6]. PBAT is a 100% biodegradable thermoplastic aliphatic–aromatic co-polyester, obtained by poly-condensation, to date, from fossil resources. Biodegradation of PBAT is recorded to fully take place in composting conditions in 45 days [7], with potential wide use in agriculture in the form of mulch films [8, 9] thanks to a series of remarkable properties, including high flexibility and elongation at break and good thermal behavior, that are comparable to those of low-density polyethylene (LDPE) [10]. On the other side, the main downsides are represented by its high cost [11] and high water–vapor permeability [12].

Since bioplastics properties are not always competitive to those of conventional fossil-based polymers [13, 14], development of experimental methods for improving the mechanical, thermal, and rheological properties, as well as the stability of these relatively new polymers, is very important.

The realization of composite materials starting from bioplastics is the main way currently covered for the improvement and modulation, according to the needs, of functional and structural properties. In particular, among the mechanical properties, an increase in stiffness values is frequently observed [15, 16]. Even in the case of not substantial improvement of the properties, mainly caused by filler-matrix incompatibility and poor interface adhesion, such as poly(hydroxybutyrate) (PHB) filled with hollow glass microspheres [17] or poly(lactic acid) (PLA) and wood flour systems [18], the realization of biocomposites allows to decrease the total costs in the bioplastics production [14].

The most diffused fillers for bioplastics consist in particles of natural origin, in order to maintain biodegradability of the final material, such as ligno-cellulosic structures [19], like cellulose nanocrystals (CNCs) [20, 21] or nano-fibers

(CNFs) [22] as well as natural fibers [23, 24] and coffee grounds [25], or nanoclays [26, 27].

Calcium-phosphate glasses (CPGs) are inorganic phosphorous-based ceramics, whose main unit is the P-tetrahedron (PO_4^{3-}) [28], with the unique and important characteristic of being completely soluble in aqueous media, thanks to the hygroscopic nature of phosphorus pentoxide (P_2O_5) [28]. CPGs were initially developed for biomedical applications such as bone repairing and scaffolds [29] and tissue engineering, often with addition of silver(I) oxide (Ag_2O), to minimize microbial contamination [30, 31].

In this work investigations on thermomechanical and viscoelastic properties and degradation stability of composites made from PBAT and CPG microparticles were carried out. The degradation stability can be defined as the ability of a substance to resist any change in its physical and chemical properties with respect to the variation of environmental factors such as temperature, light, humidity, and microbiological conditions. Studying and testing the stability of newly developed biocomposites is important to assess their potential applications and disposal conditions compared to pristine matrix and other already existing materials.

Thermo-mechanical properties and viscoelastic behavior of polymers and composite materials can be investigated by DMA characterization: typically, thermal stability and creep resistance of biocomposite materials are positively influenced by the addition of a second phase dispersed and interacting with the polymeric matrix, thus enhancing load bearing resistance and retarding the plastic deformations [32].

Another important aspect to be investigated when working with bioplastics and biocomposites is their deterioration or aging stability. Biodegradability represents sure enough an undoubted benefit for bioplastics, although it makes them highly susceptible to degradation.

The outdoor and indoor uses of polymers expose them to daylight, humidity, temperature, and other climatic conditions that can reduce their durability. Nevertheless, environmental weathering can require very long exposure times, which are unacceptable on an industrial scale.

To determine more rapidly the effect of ultraviolet (UV) radiation, heat, and moisture on the physical, chemical, and optical properties of plastics, accelerated exposure tests can be carried out using specific laboratory light sources. By means of UV chambers, exposures are simulated through more controlled conditions than those found in natural environments and the tests are designed to accelerate polymer degradation, leading to failure. Relating results from accelerated tests to actual-use conditions is however very difficult because of variability in the exposure. The main modifications caused by photo-degradation are chain scission and crosslinking through Norrish I and Norrish II reactions [33], leading to a decrease in molecular weight and consequently causing loss in mechanical properties, especially a lost in ductility [33–35]. Photo-oxidation, alongside with thermal degradation (utilization of the material at high temperatures) and chemo-degradation (exposure to harsh pH conditions), are the main abiotic degradation mechanisms, that both non-biodegradable and biodegradable materials may undergo in environmental conditions [36].

Another way of testing polymer degradation is through fragmentation process, a physical deterioration according to which the material is considered degraded when pieces with dimension smaller than 2 mm are obtained. Fragmentation tests in composting conditions can safely take place on a laboratory scale, following dedicated regulations, in small reactors and with dry and clean components. This method is not aimed at determining the biodegradability of plastic materials under composting conditions: a positive outcome from the fragmentation test will require further testing to assess biodegradability and compostability.

In fact, biodegradation is a complex biochemical phenomenon carried out by living organisms present in soil, that in aerobic environment can break down the polymer chain into simpler and low-weight molecules, such as water, carbon dioxide, methane and so on as a result of their metabolism [36]. Obtaining small pieces can be considered an advancement with respect to the current biodegradation process, providing the micro-organisms with a higher specific surface to initiate the process.

In this paper, composite materials based on PBAT and reinforced with increasing concentrations of CPG, previously realized, were studied. DMA and creep analyses were performed on dog bone specimens to determine the extent of influence of the filler particles addition on viscoelastic properties of the polymer. Degradation of the biocomposites was performed on film specimens by following appropriate standards for artificial accelerated weathering and disintegration under laboratory-scale composting conditions.

Materials and Methods

PBAT, purchased in pellet form from MAgMa Spa (Italy), was utilized in the present work as the matrix of the composites.

The CPG used as filler for the composite materials was produced according to [37] and milled into particles with a size smaller than 45 μm.

LDPE (Riblene FC 39 D) as reference film was supplied by Versalis (Eni SpA, Italy).

Materials Preparation

Composites at different CPG concentrations (0, 4, 10, 20 and 40 wt%, named respectively PBAT, PBAT+4% CPG,

PBAT+10% CPG, PBAT+20% CPG, PBAT+40% CPG) were realized through a solvent casting method, described in [38]. Briefly, PBAT was firstly dissolved at room temperature (25 °C) into chloroform ($CHCl_3$—Merck-Sigma, Germany), chosen as suitable solvent for PBAT [12, 39], and then the CPG particles were dispersed in the solution.

The solution was casted and let dry under hood at room temperature (25 °C) overnight. After chloroform evaporation, composite pellets were manually obtained from the residual film. The pellets were therefore employed in the realization of specimens and films for characterizations.

The solvent casting approach was chosen as a first explorative phase since it allows to realize polymeric composites in a laboratory environment in such a quantity to thoroughly investigate the properties but maintaining feasibility in terms of solvent consumption. If the characterization of the so obtained materials gives promising results for a large-scale application, the production of the composites could be implemented through a more industrial methodology. For ecology reasons, eliminating the consumption of large quantities of solvent should be preferable, for example employing alternative compounding methods, such as twin-screw extrusion.

Test specimens of type 1BA, according to European standards UNI EN ISO 527, were obtained by injection molding, using a MegaTech H7/18-1 machine (TECNICA DUEBI, Italy). The specimens were injected at a temperature of 130 °C with a pressure of 120 bar, maintaining the mold pressurized for 5 s to allow uniform distribution of the molten material.

Films of thickness between 0.3 and 0.4 mm were produced using a Collin P 200 T press machine, with a molding temperature of 130 °C and a maintenance at 100 bar for 3 min. LDPE film was molded at 190 °C.

Prior to processing, the composites pellets were dried at a temperature of 80 °C for at least 4 h, or up to constant mass, in order to eliminate residual humidity.

Dynamic-Mechanical Analysis

Viscoelastic properties of the materials were investigated by means of DMA analysis, performed on the linear portion of the 1BA specimens using a TA Instruments Q800, in a single cantilever clamp-configuration, with three replicates for each composite material. Before being mounted in the clamp, the specimens were cut to a length that would fit properly in it.

The temperature ramp tests were performed with a frequency of 1 Hz and an amplitude of 10 µm, the temperature going from − 55 to + 55 °C with a ramp of 3 °C/min, allowing a soaking time of 15 min when the starting temperature had been reached.

The measures recorded the storage modulus (E'), the loss modulus (E'') and the damping factor, defined as the ratio between the loss and the storage modulus ($Tan\ \delta = E''/E'$), as a function of the temperature [40, 41]. Glass transition temperature (T_g) for each composite was then calculated as the temperature corresponding to the peak of the relative $Tan\ \delta$ curve [42].

Creep Test

In the creep test strain values were measured on at least two different samples for each filler concentration, in the range between − 10 and 60 °C at intervals of 10 °C, applying a cycle consisting of 10 min of isothermal soaking time, followed by 10 min of measurement under the application of a constant stress equal to 0.2 MPa.

The results were expressed plotting the creep compliance ($J(t)$) against the test time. $J(t)$ was obtained dividing the measured strain ($\varepsilon(t)$) values, recorded at each temperature, by the applied constant stress value (σ_0) [43], and expressed in $\mu m^2/N$, equivalent to 10^{-12} Pa^{-1}, according to Eq. 1:

$$J(t) = \frac{\varepsilon(t)}{\sigma_0} = \frac{\varepsilon(t)}{0.2 \times 10^6 Pa} \quad (1)$$

Accelerated Weathering Test

Accelerated aging behavior was tested in a QUV Accelerated Weathering Tester (Q-LAB), according to the ASTM D 4329 standard, applying the G154 cycle.

Two sample films for each concentration with dimensions of 5×5 cm^2 were used for the aging test. Two samples of LDPE were also tested as reference. All samples were mounted on a sample holder and exposed to a combined cycle of UV radiance, high temperature and humidity. Precisely, the test cycle consisted in two main steps: 320 min of exposure to an UV radiance value of 0.68 W/m^2 at a wavelength of 340 nm and at a temperature of 60 °C, followed by 160 min of exposure to water vapor at a temperature of 50 °C, with the UV lamps off. In the first step, the UV conditions aim to best simulate noon summer sunlight exposure in the critical region from 365 nm down to the solar cut-off of 295 nm, with a peak emission at 340 nm. At the end of the daily cycle, the sample holders were removed from the machine and stored in a closed box to prevent uncontrolled effects due to the residual heat and humidity inside the chamber. The samples were subjected to the test cycle 5 days a week, alternating with 2 days of treatment interruption. To ensure uniform treatment, the position of each specimen was varied from the starting position each week.

According to the standard, the duration of the test was considered sufficient when "a defined change in a material property" had occurred, which in this case resulted to be 4 weeks.

Every week, the samples were dismounted and analyzed by Fourier-transform infrared spectroscopy (FTIR), optical microscopy and CIE *L*a*b** colorimetry, in order to investigate any changes in the molecular structure and in the visual appearance.

At the end of the test period, scanning electron microscopy (SEM) images of the surface of both as prepared and weathered samples were taken and energy dispersive X-ray spectrometry (EDS) was carried out on the same samples.

Disintegration Test

Disintegration test under composting conditions was carried out following the EN ISO 20200 standard. For this test, three film samples of 2.5×2.5 cm^2 were cut for each PBAT-based material and for LDPE as a non-degradability reference. The composting reactors consisted of polypropylene (PP) containers in which a hole of 5 mm in diameter was performed to allow air circulation and gas exchange. Dry synthetic solid waste was prepared as described in the standard with the following composition: 40 wt% of sawdust (purchased from OBI Italy), 30 wt% of rabbit-feed (Vitakraft, Germany), 10 wt% of ripe compost (Punta allo Zero S.r.l. for Coop, Italy), acting as inoculum, 10 wt% of corn starch (Unilever, Italy), 5 wt% of sugar (MAXI S.r.l., Italy), 4 wt% of corn seed oil (Oleificio Salvadori S.r.l., Italy) and 1 wt% of urea (supplied by Merck-Sigma, Germany). The components were mixed, then deionized water was added until reaching a wet content of 55%. All the polymeric samples were dried at 40 °C to constant mass, then weighed and the masses recorded individually. Four samples from each material were buried together in one reactor, using an iron mesh as support. The amount of wet synthetic solid waste used in each reactor was enough to allow a ratio of the test material mass to the wet synthetic waste mass equal to 0.5%. Reactors were weighed and the total masses recorded previously to put them into an ISCO NSV 9090 oven at 58 ± 2 °C. Following the methodology described in the standard, the reactors were periodically weighed, the water content restored, and the compost mixed. The overall test duration was 88 days.

For the purpose of monitoring the fragmentation process, every week the samples were recovered, rinsed with deionized water, dried overnight at 40 °C and weighed. Pictures of the appearance of the films were taken with an optical microscope.

The degree of disintegration (D) was calculated through Eq. 2 as mean of the values of three samples:

$$D = \frac{m_i - m_r}{m_i} \times 100 \tag{2}$$

where m_i is the initial dry mass of the test material and m_r is the residual mass at the time of the measurement. D values have been reported in a graph against time, expressed in days.

To validate the test, the variation in D values (ΔD), calculated with Eq. 3 taking into account three replicates for each material, according to the standard requirement, shall not exceed 10%:

$$\Delta D = \frac{D_{max} - D_{min}}{\overline{D}_i} \tag{3}$$

where D_{max} and D_{min} are, respectively, the maximum and minimum values of D and $\overline{D}_i$ is the mean value of the three.

After the sixth week, the measurements were repeated every 2 weeks, to prevent excessive deterioration caused by the manipulation of the samples.

Dry mass (DM) of the compost material before and after the test was calculated by drying two samples of known volume at 105 °C (ISCO NSV 9090) to constant mass. The result was expressed as a percentage of the total mass of the sample divided by 100.

The samples of dried compost were then calcined at 550 °C for 8 h (LKN 75, Nannetti), let cool overnight and weighed, repeating the process until constant mass was reached. The volatile-solids (VS) content, corresponding to the mass loss, for each sample was calculated by subtracting the residual mass obtained by the calcination from the total dry solids content and expressed as a percentage of the DM divided by 100. The VS content is an important parameter since it is an indication of the content of organic matter in the compost (ISO 20200).

The decrease in the total VS content (R) was calculated with Eq. 4:

$$R = \frac{\left[m_i \bullet (DM)_i \bullet (VS)_i\right] - \left[m_f \bullet (DM)_f \bullet (VS)_f\right]}{\left[m_i \bullet (DM)_i \bullet (VS)_i\right]} \times 100 \tag{4}$$

where m_i is the initial mass of the wet synthetic waste introduced into the reactor, m_f is the final mass of the compost, $(DM)_i$, $(VS)_i$, $(DM)_f$ and $(VS)_f$ are the initial dry mass, the initial volatile-solids content, the final dry mass, and the final volatile-solids content of the synthetic waste, respectively.

Validity of the test is confirmed when R assumes values greater or equal to 30%.

At the end of the test period, a sample from the residual material of each tested specimen was analyzed with FTIR.

Colorimetric Analysis

Colorimetric analysis was carried out on weathered samples with a Spectro Connect 2.5 (Techkon, Germany), considering five measuring points on each film sample, one in the center of the sample and the other four at diagonal directions from the center.

During ageing test, CIE $L^*a^*b^*$coordinates were recorded, where L is the brightness, a values indicate red or green coloration in case they are positive or negative, respectively, and likewise b values indicate yellow or blue coloration.

The color variation (ΔE) of the different composites over time was evaluated using the relationship expressed by Eq. 5:

$$\Delta E = \sqrt{\left(L_t - L_0\right)^2 + \left(a_t - a_0\right)^2 + \left(b_t - b_0\right)^2} \quad (5)$$

where L_t, a_t and b_t are the values at the time of the measurement, while L_0, a_0 and b_0 are the initial values collected before the weathering process.

Optical Microscopy

Optical images of the samples were taken with an USB Digital Microscope equipped with the MicroCapture software, in order to obtain qualitative information on the macroscopic variation of the samples during the aging and fragmentation tests.

Scanning Electron Microscopy and Electron Dispersion Spectroscopy

The performing of SEM/EDS analysis aimed to the investigation of any changes in terms of surface aspect and chemical composition of the samples that underwent aging degradation.

SEM images were acquired using the SEM-Field Emission Gun (FEG) Nova Nano SEM 450 microscope (Fei) at different magnifications.

EDS was carried out by means of the system QUANTAX-200 (Bruker, Germany), equipped with the silicon drift detector (SDD) XFlash 6/10.

Fourier-Transform Infrared Analysis

In order to study the modifications taking place in the chemical structure of the materials during the degradation period, FTIR spectroscopy was performed by means of the Spectrum Two instrumentation (Perkin Elmer, USA) in attenuated total reflectance (ATR) mode. The parameters used for the analysis were: resolution of 4 cm^{-1}, 16 scans per measurement, wavenumber range going from 400 to 4000 cm^{-1}.

For the accelerated weathering test, two measure points at the center of the specimen were considered for each sample. Therefore, for each composite material, a set of four spectra was collected. Regarding the fragmentation test, each specimen was analyzed, obtaining a total of three spectra for each composite material. In both cases, the spectrum obtained from the mean values has been considered for the discussion.

Results and Discussion

Viscoelastic Analyses

The addition of a reinforcing phase has the effect of changing the viscoelastic properties of polymer composite. Investigation of the influence of the filler content on dynamic-mechanical properties and creep allows to define the variation of the conditions of use of new materials.

DMA

Figure 1a–c represent E', E'' and $Tan\delta$ of the tested composites, respectively.

For all the PBAT-based composites, E' (Fig. 1a) decreases overall of one order of magnitude with increasing temperature in the analyzed thermal range, showing a sharp decrease with an inflection point at around –20 °C, corresponding basically to the temperature in which the glass transition takes place [44].

Considering E' values as a function of CPG concentration at different temperatures, both below and above the T_g, E' increases with the concentration of the filler independently from the temperature considered, thus indicating a reinforcing effect due to the addition of CPG microparticles.

The reinforcement efficiency of CPG in the polymer matrix can be qualitatively represented by the slope of the fitting line obtained by reporting the reduced modulus (the ratio between the storage moduli of the composite, E', and the pristine PBAT, E'_0) as a function of the filler concentration at different temperatures. The increment of E' in the composites, compared to pristine PBAT, is more evident for temperatures above T_g, as clearly visible from the higher slope of the trend line in Fig. 2a. The reinforcing effect proves to be more efficient in the rubbery state (above the T_g) of the materials rather than in the glassy state (below the T_g).

The polymer chain mobility below the T_g is inhibited in the glassy state: only atomic bonds undergo bending and stretching vibrations, hence the further stiffening is a positive but sparingly effective achievement.

In the rubbery state, on the other hand, the viscosity of the polymer generally decreases [45], activating the viscous flow of the polymer chains and therefore worsening the mechanical properties. The filler particles have a role in preventing the intermolecular movements and limiting the decrease of the mechanical properties with increasing the temperature. The realization of highly filled composites can therefore be seen as a way of broadening the temperature range of composite applications compared to the unfilled PBAT polymer.

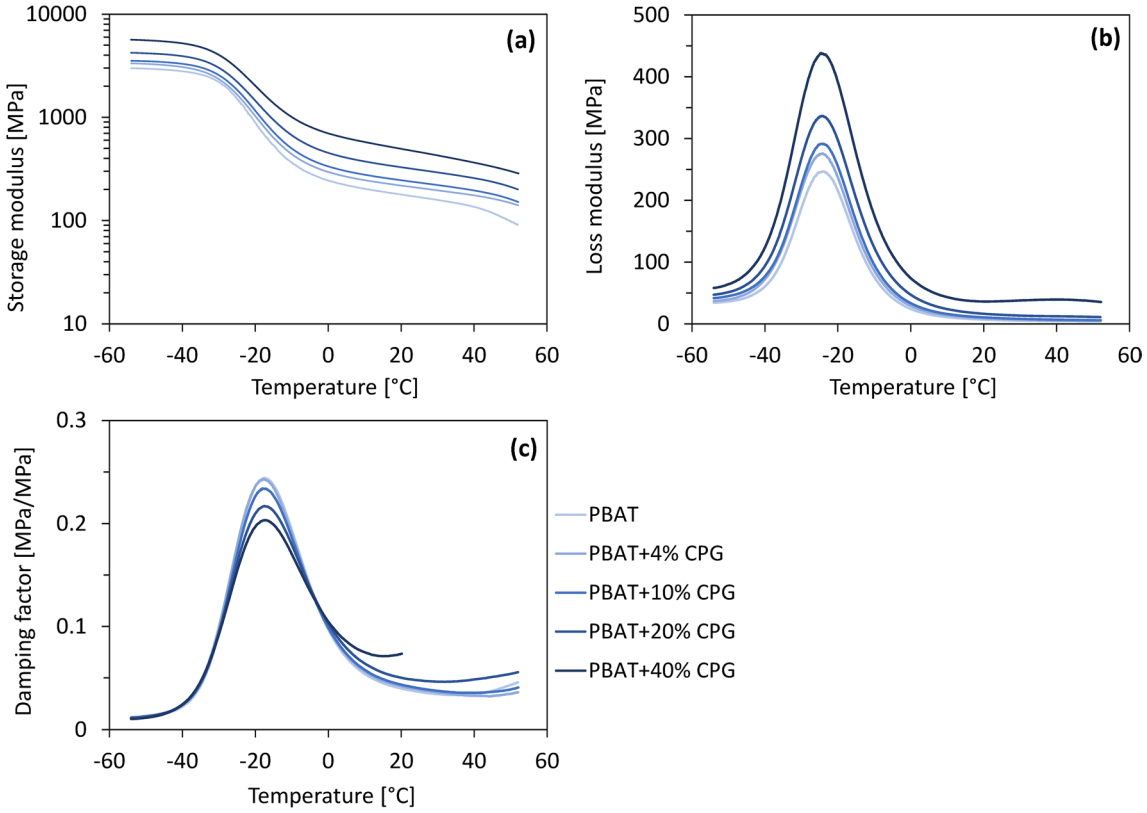

Fig. 1 Storage modulus (**a**), loss modulus (**b**) and damping factor (**c**) of the PBAT+CPG composites

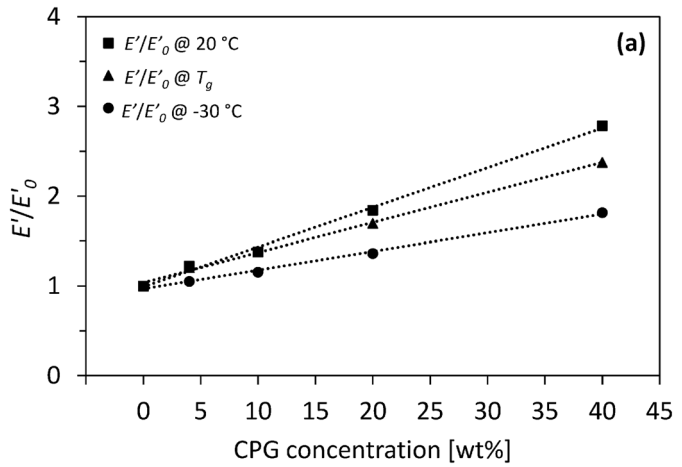

(b)

Temperature [°C]	E'/E'_0 slope
-30	0.021 ± 0.001
T_g	0.034 ± 0.001
0	0.047 ± 0.002
20	0.044 ± 0.002
40	0.041 ± 0.002

Fig. 2 Normalized increment in storage modulus (**a**) and angular coefficients of the trends (**b**)

Additionally, when considering temperatures above the T_g in the rubbery plateau (approximately between 0 and 40 °C), the reinforcing effect appeared to be quite constant (Fig. 2b), so at a given value of applied stress composite materials can be used in a wider thermal range than unfilled PBAT.

The results of E' trend are in line with the stiffening effect obtained by other authors who studied dynamic-mechanical properties of biocomposite systems with natural fibers as reinforcing agents. The stiffness of the composites increased in comparison to the neat matrix with a more pronounced increment above T_g [32].

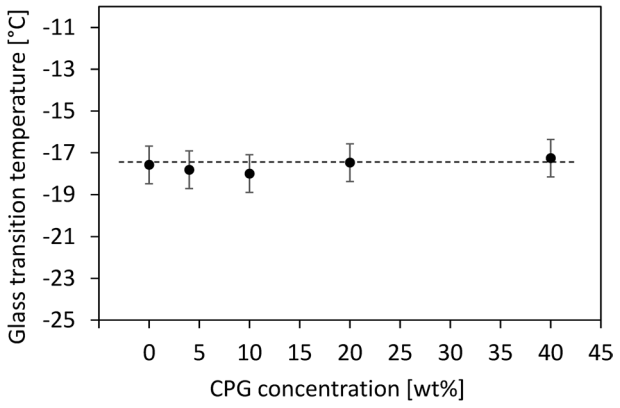

Fig. 3 Glass transition temperature as a function of filler content (the dashed line is a guide to the eye)

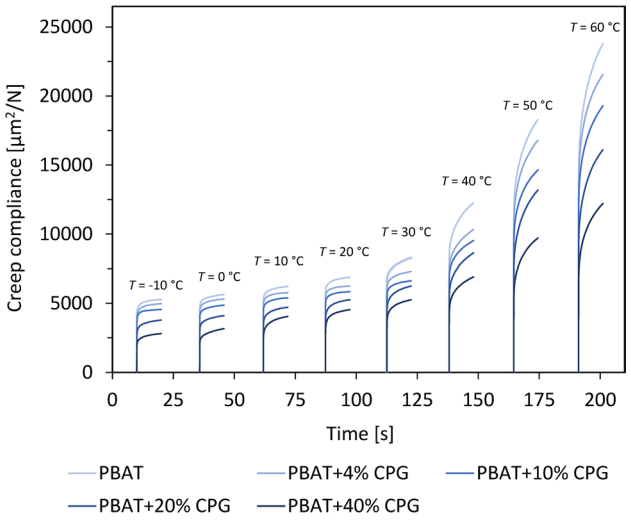

Fig. 4 Creep compliance of bare PBAT and PBAT+CPG composites at different test temperatures

E″ values (Fig. 1b) were collected to calculate *Tan δ*. *Tan δ* curves (Fig. 1c) show a peak decreasing in intensity as the CPG concentration in the composites increases without a corresponding change in temperature. This behavior can be explained considering the increment of interaction between the filler particles and the matrix, thanks to a wider interfacial area [46–48]. On the other hand, the absence of variation in the intensity and position of *Tan δ* has been interpreted in other polymer-based systems as evidence of a poor interaction between the polymer matrix and the filler, especially for nanostructured fillers for which aggregation and phase separation phenomena are more probable [49].

The values of T_g, considered as the temperature corresponding to the peak in *Tan δ* curves and represented as a function of filler concentration in Fig. 3, did not show a significant trend with increasing the filler content. More in detail, the T_g values for the different composites are not significantly different, all falling within the experimental standard deviation.

The constant trend of T_g suggests that the interaction between the matrix and the filler is limited to a good adherence without the creation of a strong chemically bonded interphase layer [50], allowing however to maintain the thermal stability of the composite. When a stronger interphase is created, an increase in T_g is usually observed [47, 51]

Creep

Figure 4 reports creep compliance values for the tested materials as a function of test time at each operating temperature.

The Burger's model, a series combination of the Maxwell's and Kelvin-Voigt's elements [52, 53], can be used to explain the experimental creep results. According to Burger's model, the creep behavior of polymer materials can be quantified by the creep compliance, *J(t)*, and characterized by three different stages: the first stage is the instantaneous elastic response ($J_1(t)$), the second stage is the retarded elastic response ($J_2(t)$) and the third stage is the viscous flow ($J_3(t)$), mathematically represented by Eq. 6:

$$J(t) = J_1(t) + J_2(t) + J_3(t) = \frac{\sigma_0}{E_1} + \frac{\sigma_0}{E_2}\left(1 - e^{-\frac{t}{\tau}}\right) + \frac{\sigma_0}{\eta_1}t \quad (6)$$

where E_1 = Maxwell's spring constant, E_2 = Kelvin-Voigt's spring constant, η_1 = viscosity of Maxwell's dashpots, η_2 = viscosity of Kelvin-Voigt's dashpots and $\tau = \eta_2/E_2$ = characteristic relaxation time, i.e., the time required to generate 63.2% of deformation in the Kelvin-Voigt's units.

The results show that the creep compliance reduced at each tested temperature when the CPG content increased. This behavior can be explained by the reduction of the instantaneous elastic response, presumably determined by an increase in the spring constants of Maxwell (E_1) and Kelvin-Voigt (E_2). The reinforcing effect that the CPG particles exert on the PBAT polymeric matrix is responsible for the increase in the creep resistance and the amplification of the elastic behavior of the material. At a higher temperature, the creep compliance of each composite material greatly increased and, as a result, the creep strain accelerated, because the retarded elastic response and the viscous behavior of the composite increased at the highest level. In fact, as the temperature increases, the viscosity of the polymeric matrix decreases, resulting in the decrease of the viscosity η_1 of the Maxwell's element and in the decrement of the relaxation time in the Kelvin-Voigt's element, which depends on the viscosity η_2.

A reinforcing effect in terms of creep behavior is frequently found in composite systems, such as bioplastics

filled with natural fibers [15, 18] and polyamide 66 with nanoclay [54].

Degradation Stability

Beside investigating the composites behavior in terms of modification of the conditions of use, as a function of filler content, this work aims, on the other side, to investigate end of life properties of the realized materials. In this way, a more complete characterization can be achieved.

Accelerated Weathering Test

PBAT-based composites stability to weathering agents was tested on film samples with accelerated aging analysis.

Artificial accelerated weathering aims to simulate in a reduced period of time the effects of environmental conditions, such as sun exposure, by irradiating the samples with UV light at temperatures above room temperature and in presence of high humidity. Aging can cause irreversible modification in the properties of polymers, and the most common effects of weathering include discoloration, embrittlement, tackiness, and loss of mechanical properties [55].

Colorimetric Analysis Changes in color ΔE have been calculated through Eq. 5 each week for each composite. ΔE values of each composite material have been plotted against the elapsed time expressed in weeks, then fitted with a linear equation (Fig. 5).

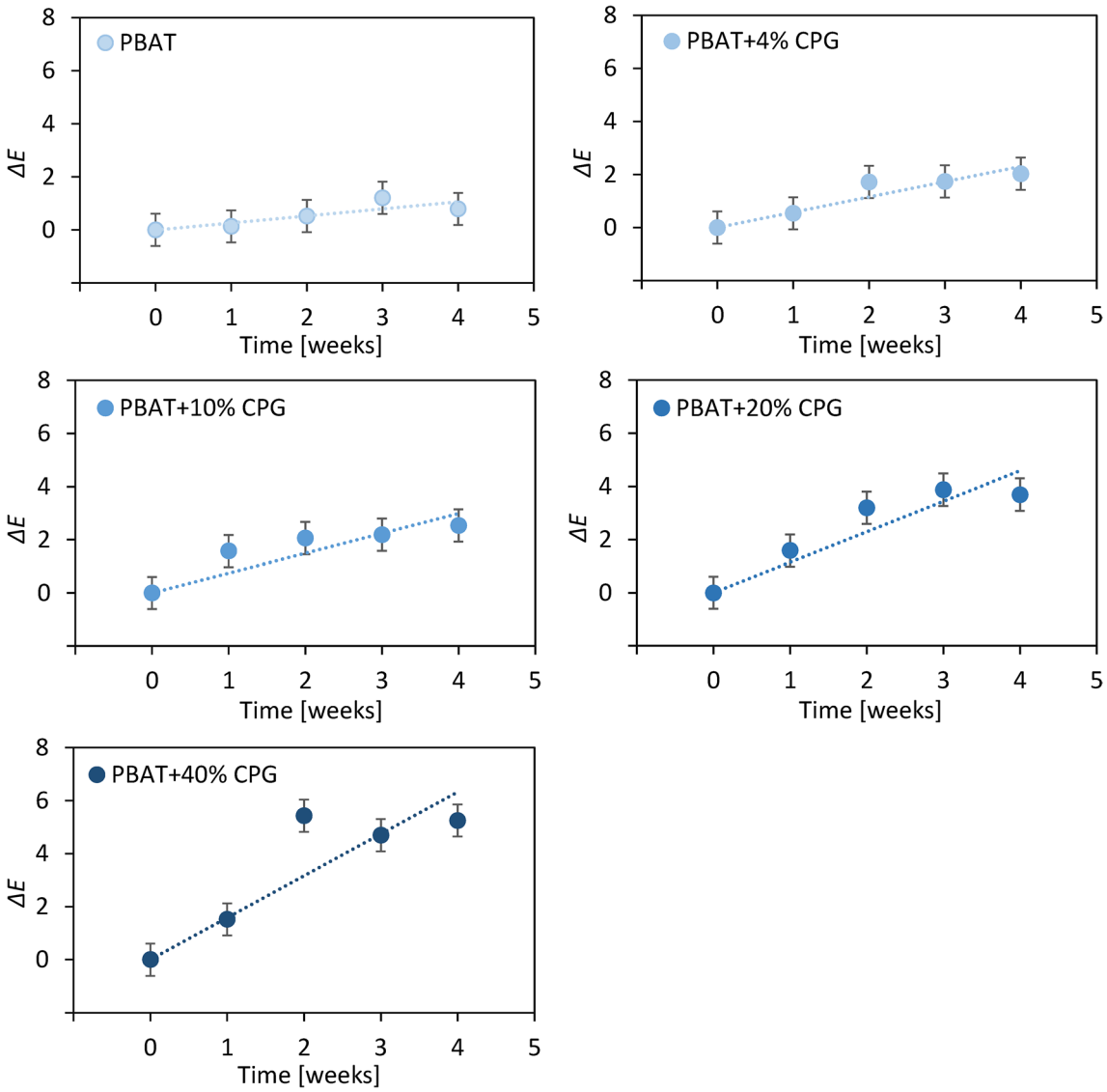

Fig. 5 Color variation of the composites over time. The round points represent the experimental data, while the dotted lines are the linear fitting curves

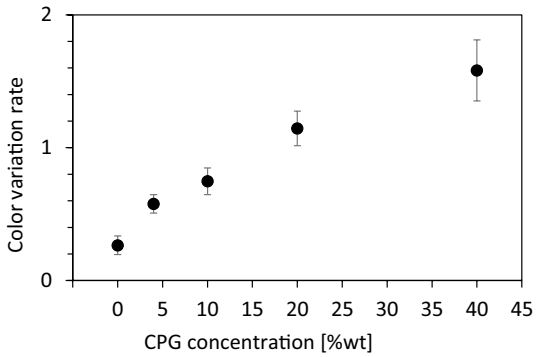

Fig. 6 Color variation rate as a function of filler content

The angular coefficient of the fitting lines, which represents the color variation rate, clearly increases as the concentration of CPG increases. These values are reported in Fig. 6 as a function of the CPG concentration, showing higher and higher values with the growth of filler content. This behavior means that, as the concentration of CPG increases, the composites undergo a greater change in color, in particular a tendency to yellowness corresponding to a faster degradation of the materials [56].

Digital microscope pictures (Fig. 7) show the change in the composite specimen appearance with the test progression: the composites with a high concentration of glass microparticles can be noted to undergo multiple fractures while the exposure proceeds, becoming more brittle and difficult to handle than the untested samples. This behavior indicates a certain deterioration degree of the material, the causes of which will be investigated below on the basis of the microscopic and spectroscopic characterization results.

PBAT+20% CPG specimens first showed a beginning of cracking during the second week of test, only visible in backlight, followed by macroscopic cracking at the third week (Fig. 7i). PBAT+40% CPG started cracking during the third week as well (Fig. 7ii), and then PBAT+10% CPG in the last week of test. At the end of the fourth week, the aging of the specimens loaded with 40 wt% of filler was extended enough to make their removal and repositioning after analyses rather complex: this fact determined the end of the test period. LDPE, that was taken as a reference for a non-degradable material, did not exhibit visible signs of deterioration.

SEM The brittle behavior could be explained by the analysis of the surface microstructure of the specimens, investigated by means of SEM. Figure 8 represents the surface morphology of the composite materials before the weathering test (on the left of Fig. 8) and at the end of the testing period (on the right of Fig. 8). In the SEM images of unaged samples, the grey portion represents the polymeric matrix and the white bodies scattered throughout it represent the filler particles. SEM images are obtained by acquiring backscattered electrons for compositional information, being sensitive to the atomic number of the atoms interacting with the electrons. Hence the higher contrast particles present in sample microstructure can be identified as inorganic phosphorous-

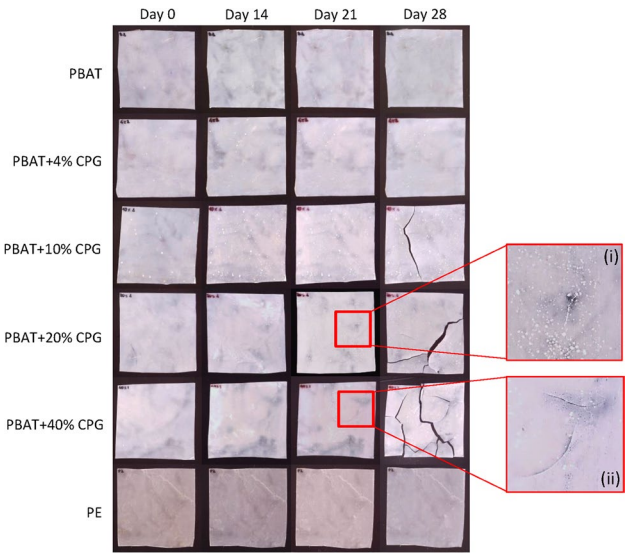

Fig. 7 Digital microscope pictures of PBAT+CPG composites and LDPE over time during the weathering test. Details (i) and (ii) represent cracking on PBAT+20% CPG and PBAT+40% CPG samples, respectively, at the third week of test

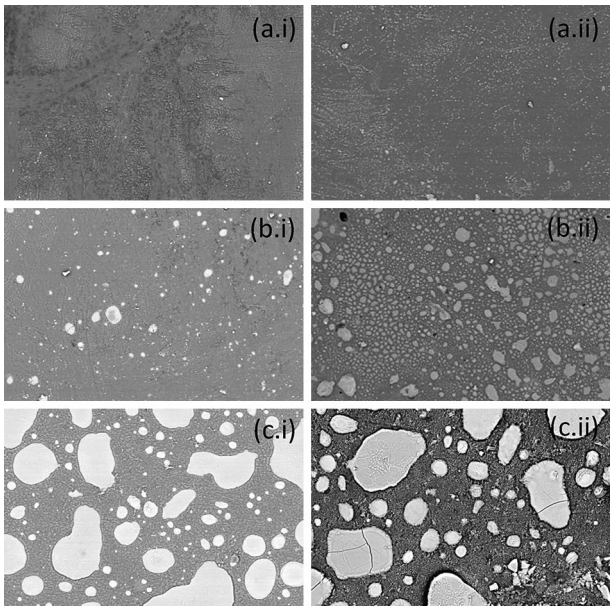

Fig. 8 Surface microstructure of PBAT (**a**), PBAT+10% CPG (**b**), and PBAT+40% CPG (**c**), as representative samples, before (i) and after (ii) 4 weeks of weathering test

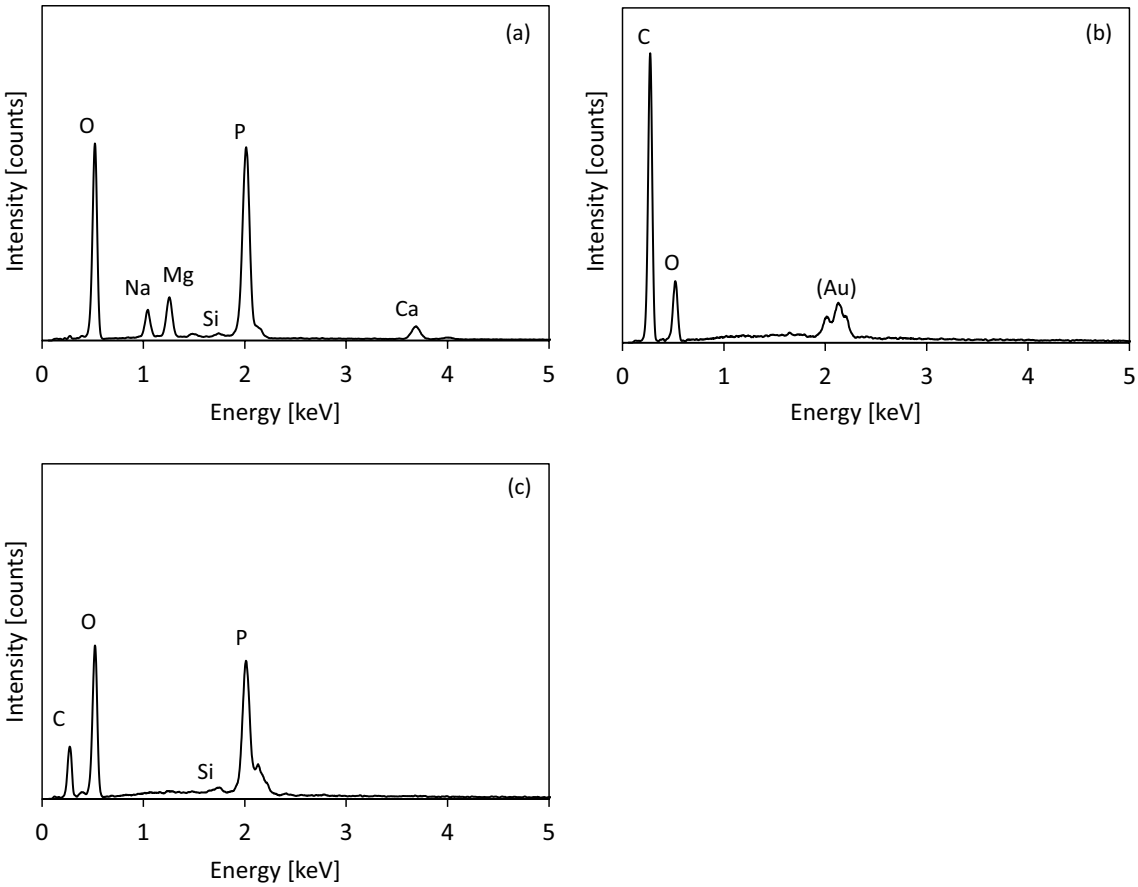

Fig. 9 EDS analysis on glass particle in unaged specimen (**a**), on PBAT surface of unaged specimen (**b**) and on a generic point of aged specimen surface (**c**)

based compounds, heavier than the carbon-based polymer matrix and therefore with a higher electron scattering.

Comparing the material microstructures before and after the test, it is possible to assume that, due to its hydrophilic nature, the CPG absorbed the water vapor during the second step of the test cycle, dissolving and forming a thin layer on top of the PBAT matrix. During the night between two consecutive test days, this glass layer dried out, covering the whole sample surface, and resulting in a more brittle and stiffer phase on top of the polymer film surface. Furthermore, the polymer itself can be involved in the absorption of water, that in the case of natural weathering comes from rain or environmental humidity, followed by drying, with repeated swelling and contraction cycles. The repetitive process, over the testing period, caused stresses that concentrated on the surface of the specimens around and across the glass areas leading them to crack, thus influencing the entire composite structure [56], which appeared with a more rigid and brittle macroscopical behavior and confirming what previously observed by digital images in Fig. 7.

By paying particular attention to the images of the samples after the aging process, image contrast is still clearly visible between the matrix and the filler, but everything shows a grey tone, rather than highlighting bright areas corresponding to the CPG microparticles on a grey background, confirming the hypothesis just explained for the glass dissolving and spreading on the specimen surface. As further evidence to this observation, EDS results will be discussed in the next Section.

EDS EDS analysis on unaged specimens was performed on two measuring points: the first on a glass particle and the second within the PBAT matrix area, the spectra of which are represented in Fig. 9a and b, respectively. In Fig. 9a only the peaks characteristic of the elements constituent the CPG are reasonably detected, such as oxygen, phosphorus, calcium, magnesium, sodium and silicon, and analogously in Fig. 9b carbon and oxygen are the only peaks distinctive of the PBAT matrix. The appearance of a spurious gold-related peak is due to a nanometric layer of metal applied on the specimen to make it conductive and to avoid charge accumulation during the test. Considering now the spectrum of a

specimen after the weathering process (Fig. 9c), the simultaneous presence of peaks ascribed to both glass filler and polymeric matrix, in a generic point on the surface of the specimen, corroborates the assumption made on the behavior of the CPG particles previously described.

FTIR Structural modifications of the materials after the weathering test were analyzed by means of FTIR spectroscopy: changes in the spectrum indicate modifications in the chemical structure of macromolecules as a consequence of the weathering process, mainly characterized by humidity and UV radiation exposure. Due to the nature of bioplastics, especially for polymers obtained from poly-condensation such as PBAT, water can be responsible for the actual chemical degradation by triggering hydrolysis reactions that lead to the breakdown of the polymer chain.

Because of its intrinsic high energy, UV radiation (wavelength < 400 nm) is one of the main sources of degradation of polymers, by photochemical reactions [56]. Indeed, the UV component of sunlight consists in photons with enough energy to split inter- and intra-molecular bonds [55].

With the aim of comparing the FTIR spectra of each composite at different times of measure, data have been normalized to the highest peak at 725 cm^{-1}, characteristic of aromatic ring out-of-plane bending, which has been assumed not to be susceptible to oxidation. The wavenumber coordinate of this peak is shifted to a lower value (generally its presence is at around 830 cm^{-1}), due to conjugation interaction between the aromatic ring and the ester groups of the terephthalate unit [57].

Characteristic peaks of PBAT-CPG composites are described in Table 1 and spectra of PBAT and PBAT+CPG composites at different filler contents are reported in Fig. 10. CPG does not influence the structure of the polymeric matrix: PBAT-related peaks are not modified, and CPG presence is detectable mainly through the band at 520 cm^{-1}, characteristic of phosphorus-oxygen bond, whose intensity increases with the content of the filler in the composite [30, 31, 58, 59].

For pristine PBAT (Fig. 10a), FTIR spectra over aging time do not show considerable modification, with only the formation of a very weak band between 3000 and 3700 cm^{-1} which identifies the formation of hydroxyl groups. Since no other evident modification took place, the presence of (OH^-) is attributed to the absorption of water on the surface of the samples [9].

In the case of PBAT composites (Fig. 10b–e) changes are particularly evident. The most important modification is the formation of a wide band at 3000–3700 cm^{-1}, characteristic of (OH^-) bond, together with a noticeable decrease of the intensity of the (C=O) and ((O=)C–O) bonds of the ester group respectively at 1710 and 1260 cm^{-1} [9, 60], in turn supported by the formation of a shoulder to the peak at 1645 cm^{-1}, distinctive of (C=O) bond in carboxylic acids involved in the formation of intermolecular hydrogen bonds [61]. This observation suggests the hydrolysis of the ester group in the main polymer chain, with formation of alcohol and carboxyl functionality by addition of a water molecule. The combined action of UV radiation and water molecule absorption leads to the macromolecule breakdown with the formation of a free acid group, which can interact with other molecules, with the formation of hydrogen bonds causing a shift towards lower wavenumbers in the carbonyl absorption peaks [61].

Beside the degradation of the polymer chain, the intensification in the hydroxyl band may be also due to the formation of hydroxyl groups in the glass, thanks to its hydrophilic nature. In fact, this behavior becomes more and more evident for composites that are more concentrated in CPG.

On the other hand, the formation of a peak at 2352 cm^{-1}, ascribable to the stretching of (P-OH) bond [61], is observable and its intensity increases as the concentration of phosphate glass and the testing period increase. The same behavior is shown by the band at 520 cm^{-1}, characteristic of bending vibration of the same bond. The formation of the peak at 2352 cm^{-1} could be explained by the mechanism for which the glass content solubilizes into the surface absorbed water during the second step of the test cycle, forming a thin and more homogeneous layer on top of the specimen surface, as already presented in the SEM images.

Analyzing the LDPE spectra (Fig. 10f), the main peaks (the symmetric and asymmetric CH_2 stretching at 2915

Table 1 Characteristic IR absorption peaks of PBAT-CPG composites

Wavenumber [cm^{-1}]	Description
2800–2900	Adipate and 1,4-butandienol ($-CH_2-$) groups symmetric and asymmetric stretching
1710	Adipate and terephthalate carbonylic (C=O) stretching in ester group
1577–1504	Aromatic benzene ring (C=C) bond stretching
1267–1250	((O=)C–O) bond asymmetric stretching in ester group
1110	((C–)C–O) bond stretching in 1,4-butanediol group
1014	Aromatic benzene ring (C–H) bond in-plane bending in terephthalate unit
725	Aromatic benzene ring (C–H) bond out-of-plane bending in terephthalate unit
520	P–O bond bending

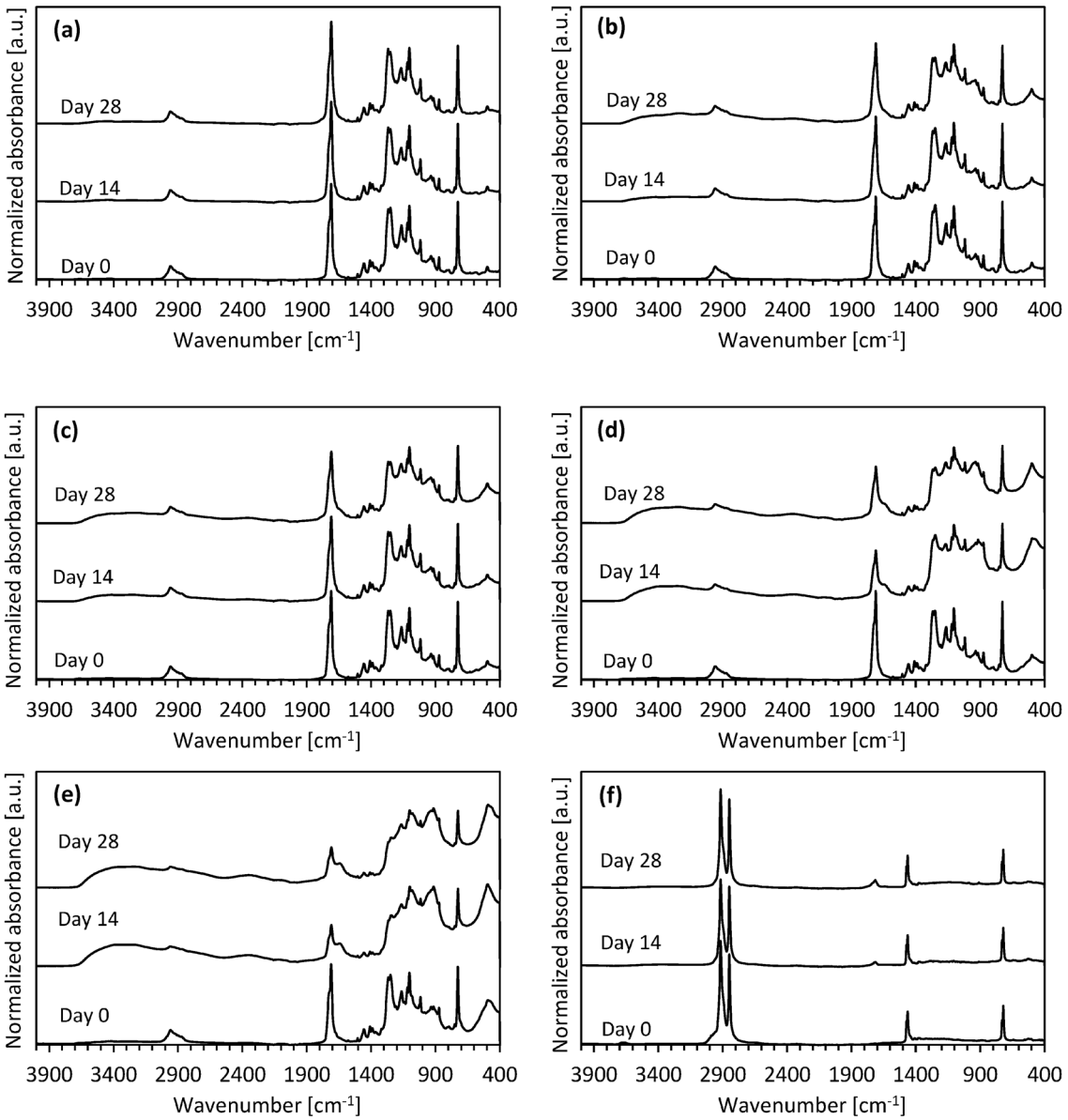

Fig. 10 PBAT (**a**), PBAT+4% CPG (**b**), PBAT+10% CPG (**c**), PBAT+20% CPG (**d**), PBAT+40% CPG (**e**) and LDPE (**f**) FTIR spectra over time during the weathering test

and 2848 cm^{-1}, the bending deformation at 1471 and 1462 cm^{-1} and the rocking deformation of the carbon chain at 730–719 cm^{-1}) are not affected by the aging process [62]. The most important modification of the spectrum over time is the formation and increment of a peak in the region between 1700 and 1800 cm^{-1}, indicating the formation of carbonyl groups, suggesting therefore a degradation by photooxidation of the polyethylene chain structure [55, 63, 64]. A very weak increase of intensity in the region of hydroxyl groups can be observed. Overall, compared to the degradation of PBAT-CPG composites, the aging effect on LDPE samples can be considered negligible.

Disintegration Test

A first step to assess degradability of polymeric materials can be made by determining the degree of disintegration of samples under composting conditions. The ISO 20200 standard offers an easy-to-reproduce methodology for laboratory-scale tests. This method does not aim to the determination of biodegradability in composting conditions and, especially, further testing is necessary to claim compostability.

Physical Appearance Visual inspection of the samples can be easily carried out and reported with the use of optical

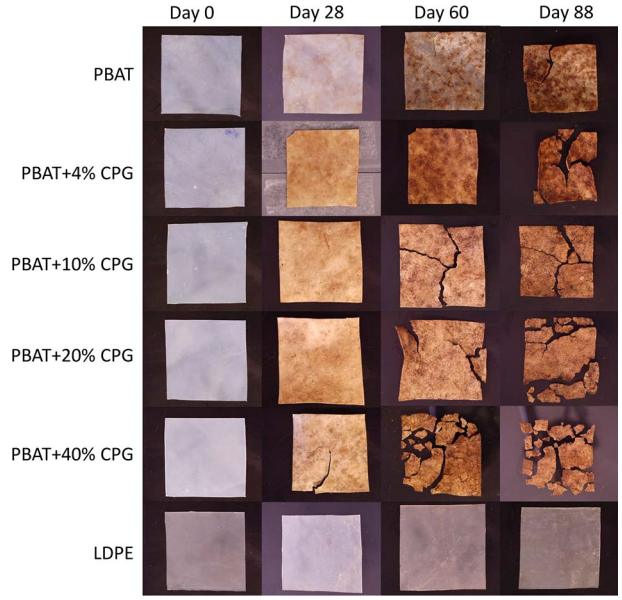

Fig. 11 Degradation of PBAT, PBAT-CPG composites and LDPE over time

microscopy. In Fig. 11 a comparison of the macroscopical specimen morphology is represented for the samples at the beginning of the test and after 28, 60, and 88 days.

As in the case of accelerated weathering, LDPE did not show visual signs of deterioration, not even at the end of the test, while PBAT and the composites underwent a significant change in appearance. The change in color affected in different ways PBAT and the composites. PBAT assumed a compost-like brown color maintaining a partial transparency. The composites assumed a brown color that intensified with the proceeding of the test, like PBAT, but turned opaque by the second week of test.

The specimen fragmentation increased with the filler content and the time, the materials resulting more and more fragile every time they were took out from the compost. Also, with the ongoing of the test, after being recovered, rinsed, and dried overnight at 40 °C, the films became more and more brittle and difficult to manipulate.

Compost Aspect The variation of the compost aspect was monitored over time as a standard requirement.

Regarding the odor monitoring, at the beginning of the test, a mixed smell of the sawdust and the rabbit-feed was prevalent, the seventh day a strong ammoniacal odor started forming and lasted for about 2 weeks, slowly degrading into a mild odor that persisted for the whole test duration.

The color of the compost varied from a light brown, when the dry synthetic waste was first mixed with deionized water, to a very dark brown when ammoniacal odor was present, corresponding to a maturation phase. As a matter of fact,

Fig. 12 Appearance of the compost during the 3rd week of test

during this time, mold spots and bacterial activity evidence, like gas production, were observable on the surface of the compost (Fig. 12).

The detected variations in both color and odor are in accordance to what is described in ISO 20200 standard.

FTIR Figure 13 represents the FTIR spectra of the samples before and after the fragmentation test, normalized to the peak at 725 cm^{-1} characteristic of aromatic ring out-of-plane bending, as done previously for FTIR spectra of the samples subjected to accelerated weathering test.

When comparing the spectra after the test period to the ones of the untested samples, the main characteristic is a substantial de-structurization of the spectrum: in the fingerprint region (1200 to 700 cm^{-1}), the peaks appear different after 88 days of fragmentation, with the absorbance values homogenized to a medium intensity, making it difficult to identify representative signals, and suggesting a chemical deterioration in the polymer molecule.

Again, it is noticeable the formation of a wide band characteristic of (OH^-) bond at 3000–3700 cm^{-1}, due to the absorption of water by the film, superposed with a peak at 3278 cm^{-1}, which is attributable to the amide bond of urea [61], as a residual on the surface of the samples coming from the compost composition.

A big difference with the spectrum after aging (Fig. 10) is the decrease in intensity of the ester carbonylic linkage (C=O) stretching peak (1710 cm^{-1}), compatible with the complete deterioration of the polymer chain not into monomers but into simple molecules by the metabolic action of microorganisms in the soil.

As a matter of fact, the degradation of PBAT in soil in controlled conditions is due to two main processes: enzymatic and non-enzymatic degradation, the first carried out by aerobic microorganisms, like bacteria, fungi, and algae, and the second by hydrolytic process [11, 65]. Often, abiotic

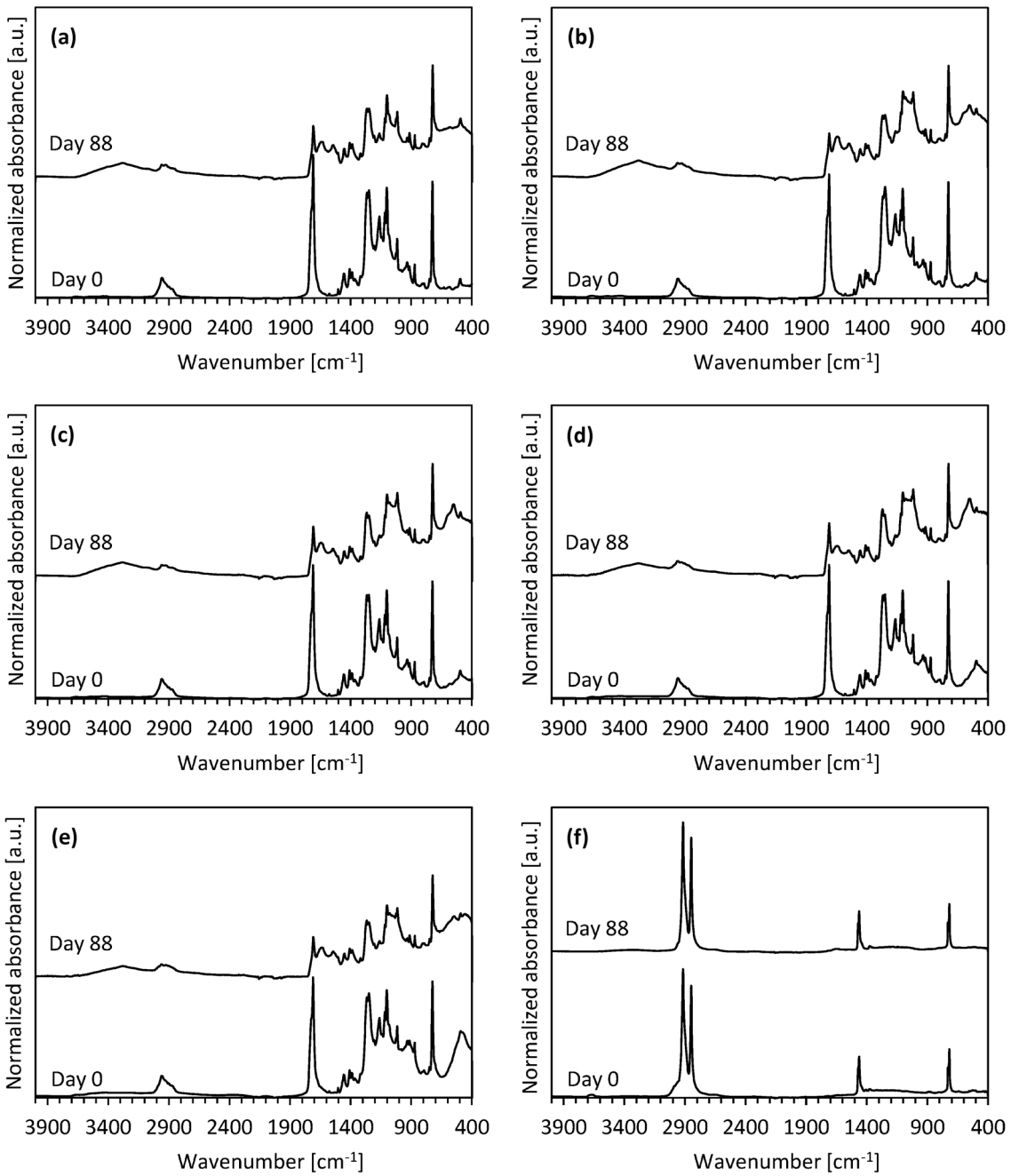

Fig. 13 PBAT (**a**), PBAT+4% CPG (**b**), PBAT+10% CPG (**c**), PBAT+20% CPG (**d**), PBAT+40% CPG (**e**) and LDPE (**f**) FTIR spectra at the beginning and at the end of the fragmentation test

hydrolysis acts as a precursor for microbial degradation causing depolymerization, that is the scission of the polymer chain into molecules of lower molecular weight that are easier for the microorganisms to utilize as sources of carbon for their metabolism [66].

The comparison of LDPE spectra before and after the test confirmed, once again, that it did not face any kind of deterioration, as supposed from visual inspection, given both the absence of new peaks and the modification of the pre-existent ones.

Calculation of the Degree of Disintegration It was evident from visual appearance that all PBAT-CPG composite samples experienced a marked weight loss during the test.

To calculate and monitor *D*, expressed as mass loss percentage, Eq. 2 was applied every time the samples were

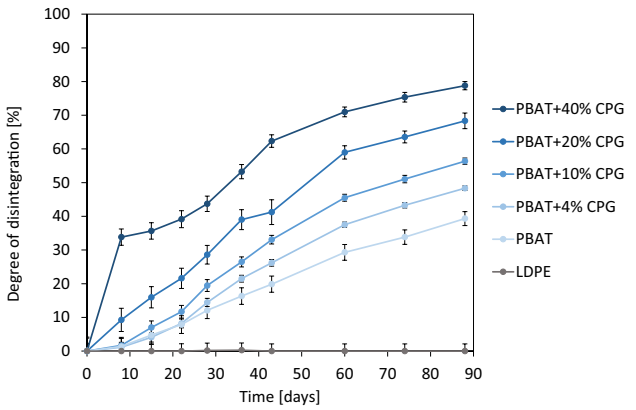

Fig. 14 Disintegration degree D of PBAT, PBAT+CPG composites and LDPE over time (the continuous lines are just a guide to the eye)

recovered from the reactors. Mean D values as a function of time, expressed in days, are reported in Fig. 14. As expected, LDPE did not deteriorate, while pristine PBAT and PBAT-CPG composites showed an increasing degradation both as a function of time and of the CPG content. In the first week of test, while the mass of neat PBAT and the composites with 4 and 10 wt% filler content remained almost constant, PBAT+20% CPG showed a first decrease in mass. PBAT+40% CPG followed a particular behavior, losing over 35% of its mass, presumably in CPG content, which dissolved in the water contained in the compost. After 14 days of test, all biocomposites assumed a homogeneous trend. At the end of the 88 days of test, the biocomposites reached a degree of disintegration between 38 and 79%, corresponding to PBAT and PBAT+40% CPG, respectively. LDPE is an oil-based non-biodegradable polymer, hence it was chosen as a reference for non-degradability, while PBAT is completely biodegradable with its degradation varying with progression of time. The addition of water-soluble CPG further increased the degradation rate as a function of the filler content. CPG particles exhibit hydrophilic behavior and the increased water absorption, at high CPG concentrations, can accelerate hydrolysis activity catalyzing the degradation and breaking of polymer chain, as similarly observed for modified-thermoplastic starch/PBAT blends [67].

CPGs completely dissolve in aqueous solutions and their solubility can be varied by changing the glass composition [68, 69]. Assuming that all CPG content had dissolved in the water contained in the compost and subtracting it from the total percentage of degradation, all composites showed a degradation of the PBAT matrix that falls within 38 and 46%. This result is congruent compared to the values of degradation reported in other PBAT degradation studies; Kijchavengkul et al. obtained, indeed, a degree of biodegradation going from 33 to 67% in 45 days, depending on the type of compost used [7].

Also, it has been reported that greater disintegration degrees can be obtained for PBAT composites previously aged through UV radiation [26].

The ratio $M_R = \frac{m_r}{m_i}$, corresponding to the mass reduction related to the initial mass of the specimen, was also calculated and reported as a function of time for the tested composites.

The M_R values, plotted against the test duration expressed in days for each composite material (Fig. 15), can be fitted with a decreasing exponential function in the form of $M_R = M_0 e^{-K_R \cdot t}$, where t is the time, M_0 represents the mass reduction at the initial time ($t = 0$) and it is imposed equal to 1, and the coefficient K_R represents the mass reduction rate or degradation rate. The data corresponding to the first 3 weeks are not considered, because that period corresponds to the maturation stage of the compost, in which only small molecules can be degraded and the decomposition process is not fully developed yet [70]. The decay trend of the

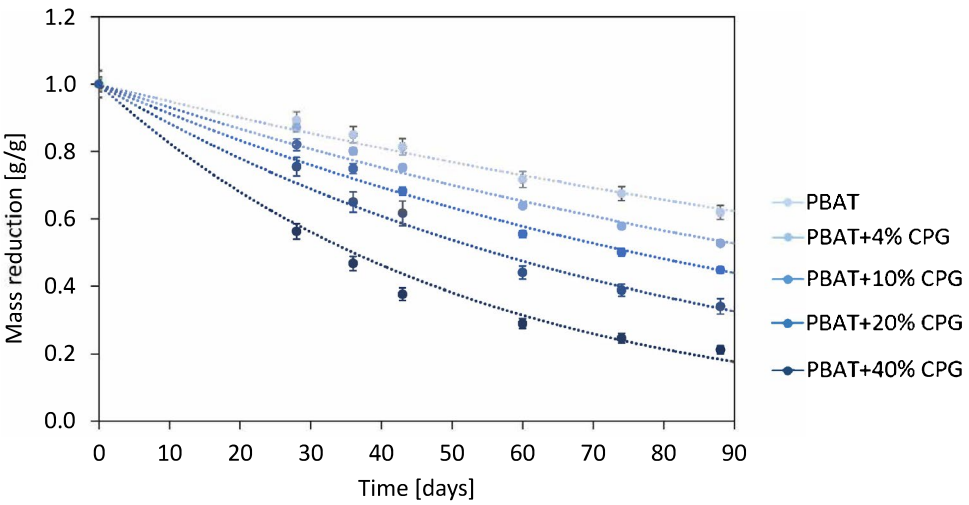

Fig. 15 The mass reduction M_R of PBAT and PBAT+CPG composites over time. The round points represent the experimental data, while the dotted lines are the fitting curves

fitting curves appears increasingly marked as the CPG content increases. In fact, the K_R values, obtained by the fitting function, increase with the CPG content and are reported in Table 2, allowing the prediction of the disintegration behavior of composite materials under aerobic composting conditions over time.

To verify the presence of a relationship between the K_R values and the CPG concentration in the composites, a statistical analysis was applied by calculating the covariance ($\sigma_{xy} = \frac{\sum_{i=1}^{n}(x_i-\bar{x})(y_i-\bar{y})}{n}$) and the correlation coefficient ($C_C = \frac{\sigma_{xy}}{\sigma_x \bullet \sigma_y}$), where x_i and $\bar{x}$ are respectively the i-th value and the average of the examined CPG concentrations, y_i and $\bar{y}$ are respectively the i-th value and the average of the K_R rates, while $\sigma_x = \sqrt{\frac{\sum_{i=1}^{n}(x_i-\bar{x})^2}{n}}$ and $\sigma_y = \sqrt{\frac{\sum_{i=1}^{n}(y_i-y)^2}{n}}$ are respectively the standard deviations of the two statistical variables under consideration. The obtained results are reported in Table 2.

σ_{xy} assumes a positive value equal to 0.076 indicating the presence of a positive interdependence between the two variables and their correlation is also strong since the C_C is equal to 0.999, a very high value and close to 1. Therefore, it is possible to state that increasing the CPG concentration in the polymer matrix actually results in the K_R increase.

Plotting K_R values as a function of the CPG concentration (Fig. 16), a linear proportionality with the filler content is observable, confirming the higher composite disintegration rate compared to the pristine PBAT. To have a quantitative relationship between CPG concentration and K_R, the simple linear regression method was applied considering respectively the CPG concentration and K_R as independent and dependent variables and setting a 95% confidence level (Microsoft Excel, USA). The statistical parameters (intercept α, slope β and coefficient of determination R^2) and relative errors, resulting from the linear regression, are shown in Table 2, while the equation of the fitting line in its complete form is represented in Fig. 16. The value of R^2 is very high indicating a very good fit of the data to the regression model, allowing the prediction of the composite disintegration behavior under aerobic composting conditions over time.

Table 2 K_R values, obtained by the exponential fitting function, and statistical parameters, extracted by statistical analysis

Sample	K_R value
PBAT	0.0052 ± 0.0002
PBAT+4% CPG	0.0070 ± 0.0003
PBAT+10% CPG	0.0090 ± 0.0003
PBAT+20% CPG	0.0122 ± 0.0004
PBAT+40% CPG	0.0204 ± 0.0007
Statistical parameters	
σ_{xy}	0.076
C_C	0.999
α	0.0052 ± 0.0002
β	0.00037 ± 0.00001
R^2	0.997

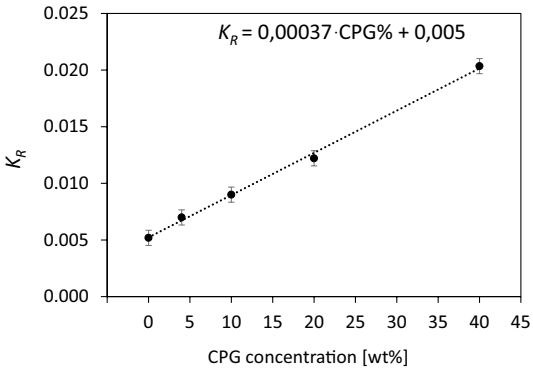

Fig. 16 Mass reduction rate K_R as a function of the CPG concentration for PBAT and PBAT+CPG composites. The round points represent the experimental data, while the dotted line is the linear fitting curve

Validity of the Test As a requisite for the validity of the test, D values should not differ by more than 10% between each tested sample. Table 3 reports the calculated final values of D for the individual samples and their relative variation.

The calculation of the decrease in volatile-solids in the compost with Eq. 4 aimed to the validation of the test. The values of two samples of compost collected from each reactor are reported in Table 4.

Being R greater than 30% in all the reactors and being the condition on the variation of D satisfied, the test can be considered valid for all the reactors.

Conclusions

The present work aimed to study the dynamic-mechanical and viscoelastic behavior of PBAT and CPG microparticles composite materials at different concentrations of

Table 3 D values and maximum relative variation

	D_1	D_2	D_3	ΔD [%]
PBAT	0.37	0.36	0.37	6.88 ± 0.07
PBAT+4% CPG	0.48	0.47	0.46	2.57 ± 0.03
PBAT+10% CPG	0.55	0.55	0.54	2.75 ± 0.03
PBAT+20% CPG	0.64	0.63	0.68	7.60 ± 0.08
PBAT+40% CPG	0.78	0.79	0.77	2.51 ± 0.03
LDPE	0.00	0.00	0.00	0.00 ± 0.00

Table 4 Calculation of the decrease in volatile-solids *R*

	m_i	m_f	$(DM)_i$	$(DM)_f$	$(VS)_i$	$(VS)_f$	*R [%]*
PBAT	188.09	105.28	0.41	0.35	0.95	0.90	55 ± 2
PBAT+4% CPG	226.79	129.39	0.40	0.34	0.95	0.90	54 ± 1
PBAT+10% CPG	251.24	144.58	0.40	0.34	0.95	0.89	55 ± 1
PBAT+20% CPG	251.28	143.80	0.41	0.34	0.95	0.90	55 ± 1
PBAT+40% CPG	298.26	179.15	0.42	0.33	0.95	0.85	58 ± 1
LDPE	234.62	131.78	0.40	0.34	0.95	0.90	55 ± 1

filler. The stability of the same materials to degradation due to accelerated weathering and to laboratory-scale composting conditions was then tested and compared to that exhibited by LDPE.

An increasing trend in the E' beside any noteworthy change in the glass transition temperature with the increase of filler content are noted. The realized composites became stiffer but did not lose thermal stability also at high CPG percentages. The same reinforcing effect was confirmed by the reduction of creep compliance: the CPG addition at increasing amounts enhanced the deformation resistance under constant stress.

The results collected from accelerated weathering of the films pointed out that, as the concentration of filler particles increased, the material became more susceptible to structural and macroscopic modifications with a marked tendency to embrittlement and deterioration as the weathering process proceeds.

Disintegration test proved an increasing deterioration trend with the filler concentration, having *D* a satisfactory value according to the followed standard. On the other hand, LDPE, taken as reference, confirms its non-biodegradable nature.

The addition of increasing amounts of CPG microparticles to a PBAT polymeric matrix allows to obtain the modulation of mechanical and viscoelastic properties. At the same time, the characteristic degradation properties of PBAT are maintained in the composites and, in turn, can be modified by the filler content accordingly to specific needs. The obtained results allow to propose PBAT-CPG composites as a sustainable alternative to thermoplastic polymers commonly in use for many fields, such as packaging and agriculture.

Acknowledgements The authors would like to thank Prof. Massimiliano Rinaldi and Prof. Eleonora Carini, Department of Food and Drug Sciences, University of Parma, and Prof. Felice Giuliani, Department of Engineering and Architecture, University of Parma, for having kindly granted the use of the instruments for the experimental characterization activity.

Author Contributions ET: Investigation, Formal Analysis, Data Curation, Writing—Original Draft Preparation; DM: Supervision, Writing—Review and Editing; DP: Investigation; CS: Supervision, Conceptualization, Methodology, Writing—Review and Editing.

Funding Open access funding provided by Università degli Studi di Parma within the CRUI-CARE Agreement. This research did not receive any specific grant from funding agencies in the public, commercial, or not-for-profit sectors.

Declarations

Conflict of interest The authors declare no conflict of interest.

Open Access This article is licensed under a Creative Commons Attribution 4.0 International License, which permits use, sharing, adaptation, distribution and reproduction in any medium or format, as long as you give appropriate credit to the original author(s) and the source, provide a link to the Creative Commons licence, and indicate if changes were made. The images or other third party material in this article are included in the article's Creative Commons licence, unless indicated otherwise in a credit line to the material. If material is not included in the article's Creative Commons licence and your intended use is not permitted by statutory regulation or exceeds the permitted use, you will need to obtain permission directly from the copyright holder. To view a copy of this licence, visit http://creativecommons.org/licenses/by/4.0/.

References

1. Andrady AL, Neal MA (2009) Applications and societal benefits of plastics. Philos Trans R Soc B: Biol Sci 364:1977–1984. https://doi.org/10.1098/rstb.2008.0304
2. Piergiovanni L, Limbo S (2010) Food packaging. In: Piergiovanni L, Limbo S (eds) Materiali, tecnologie e qualità degli alimenti, 1st edn. Springer, Milano
3. Chauhan S, Wani S (2019) Plastic pollution: a major environmental threat. IJIRT Journal 6:43–46
4. Geyer R, Jambeck JR, Law KL (2017) Production, use, and fate of all plastics ever made. Sci Adv. https://doi.org/10.1126/SCIADV.1700782
5. He D, Luo Y, Lu S et al (2018) Microplastics in soils: analytical methods, pollution characteristics and ecological risks. TrAC Trends Anal Chem 109:163–172
6. Market—European Bioplastics e.V. (2021). https://www.european-bioplastics.org/market/. Accessed 28 Oct 2021
7. Kijchavengkul T, Auras R, Rubino M et al (2010) Biodegradation and hydrolysis rate of aliphatic aromatic polyester. Polym Degrad Stab 95:2641–2647. https://doi.org/10.1016/j.polymdegradstab.2010.07.018

8. Souza PMS, Coelho FM, Sommaggio LRD et al (2019) Disintegration and biodegradation in soil of PBAT Mulch films: influence of the stabilization systems based on carbon black/hindered amine light stabilizer and carbon black/vitamin E. J Polym Environ 27:1584–1594. https://doi.org/10.1007/s10924-019-01455-6
9. Kijchavengkul T, Auras R, Rubino M et al (2008) Assessment of aliphatic–aromatic copolyester biodegradable mulch films. Part I: Field study. Chemosphere 71:942–953. https://doi.org/10.1016/J.CHEMOSPHERE.2007.10.074
10. Jian J, Xiangbin Z, Xianbo H (2020) An overview on synthesis, properties and applications of poly(butylene-adipate-co-terephthalate)–PBAT. Adv Ind Eng Polym Res 3:19–26
11. Ferreira FV, Cividanes LS, Gouveia RF, Lona LMF (2019) An overview on properties and applications of poly(butylene adipate-co-terephthalate)–PBAT based composites. Polym Eng Sci 59:E7–E15
12. Li G, Shankar S, Rhim JW, Oh BY (2015) Effects of preparation method on properties of poly(butylene adipate-co-terephthalate) films. Food Sci Biotechnol 24:1679–1685. https://doi.org/10.1007/S10068-015-0218-5
13. Peelman N, Ragaert P, de Meulenaer B et al (2013) Application of bioplastics for food packaging. Trends Food Sci Technol 32:128–141
14. Siracusa V, Rocculi P, Romani S, Rosa MD (2008) Biodegradable polymers for food packaging: a review. Trends Food Sci Technol 19:634–643
15. Nanni A, Messori M (2020) Thermo-mechanical properties and creep modelling of wine lees filled Polyamide 11 (PA11) and Polybutylene succinate (PBS) bio-composites. Compos Sci Technol 188:107974. https://doi.org/10.1016/J.COMPSCITECH.2019.107974
16. Sritham E, Phunsombat P, Chaishome J (2018) Tensile properties of PLA/PBAT blends and PLA fibre-reinforced PBAT composite. MATEC Web Conf 192:03014. https://doi.org/10.1051/MATECCONF/201819203014
17. Araque LM, de Morais ACL, Alves TS et al (2019) Preparation and characterization of poly(hydroxybutyrate) and hollow glass microspheres composite films: Morphological, thermal, and mechanical properties. J Market Res 8:935–943. https://doi.org/10.1016/j.jmrt.2018.07.005
18. Georgiopoulos P, Kontou E, Niaounakis M (2014) Thermomechanical properties and rheological behavior of biodegradable composites. Polym Compos 35:1140–1149. https://doi.org/10.1002/pc.22761
19. Giubilini A, Sciancalepore C, Messori M, Bondioli F (2020) New biocomposite obtained using poly(3-hydroxybutyrate-co-3-hydroxyhexanoate) (PHBH) and microfibrillated cellulose. J Appl Polym Sci 137:48953. https://doi.org/10.1002/APP.48953
20. Giubilini A, Siqueira G, Clemens FJ et al (2020) 3D-printing nanocellulose-poly(3-hydroxybutyrate- co-3-hydroxyhexanoate) biodegradable composites by fused deposition modeling. ACS Sustain Chem Eng 8:10292–10302. https://doi.org/10.1021/acssuschemeng.0c03385
21. Vatansever E, Arslan D, Sarul DS et al (2020) Development of CNC-reinforced PBAT nanocomposites with reduced percolation threshold: a comparative study on the preparation method. J Mater Sci 55:15523–15537. https://doi.org/10.1007/s10853-020-05105-4
22. Mukherjee T, Czaka M, Kao N et al (2014) Dispersion study of nanofibrillated cellulose based poly(butylene adipate-co-terephthalate) composites. Carbohydr Polym 102:537–542. https://doi.org/10.1016/j.carbpol.2013.11.047
23. Pereira da Silva JS, Farias da Silva JM, Soares BG, Livi S (2017) Fully biodegradable composites based on poly(butylene adipate-co-terephthalate)/peach palm trees fiber. Compos B Eng 129:117–123. https://doi.org/10.1016/j.compositesb.2017.07.088
24. Ferreira FV, Pinheiro IF, Mariano M et al (2019) Environmentally friendly polymer composites based on PBAT reinforced with natural fibers from the amazon forest. Polym Compos 40:3351–3360. https://doi.org/10.1002/PC.25196
25. Moustafa H, Guizani C, Dufresne A (2017) Sustainable biodegradable coffee grounds filler and its effect on the hydrophobicity, mechanical and thermal properties of biodegradable PBAT composites. J Appl Polym Sci 134:44498. https://doi.org/10.1002/APP.44498
26. Falcão GAM, Almeida TG, Bardi MAG et al (2019) PBAT/organoclay composite films—part 2: effect of UV aging on permeability, mechanical properties and biodegradation. Polym Bull 76:291–301. https://doi.org/10.1007/s00289-018-2385-z
27. Pegoretti A, Dorigato A, Penati A (2007) Tensile mechanical response of polyethylene-clay nanocomposites. Express Polym Lett 1:123–131. https://doi.org/10.3144/expresspolymlett.2007.21
28. Knowles JC (2003) Phosphate based glasses for biomedical applications. J Mater Chem 13:2395–2401
29. Navarro M, del Valle S, Martínez S et al (2004) New macroporous calcium phosphate glass ceramic for guided bone regeneration. Biomaterials 25:4233–4241. https://doi.org/10.1016/j.biomaterials.2003.11.012
30. Baia L, Baia M, Kiefer W et al (2006) Structural and morphological properties of silver nanoparticles-phosphate glass composites. Chem Phys 327:63–69. https://doi.org/10.1016/j.chemphys.2006.03.036
31. Baia L, Muresan D, Baia M et al (2007) Structural properties of silver nanoclusters-phosphate glass composites. Vib Spectrosc 43:313–318. https://doi.org/10.1016/j.vibspec.2006.03.006
32. Nanni A, Parisi M, Colonna M, Messori M (2021) Thermo-mechanical and morphological properties of polymer composites reinforced by natural fibers derived from wet blue leather wastes: a comparative study. Polymers 13:1837. https://doi.org/10.3390/POLYM13111837
33. Zhang T, Han W, Zhang C, Weng Y (2021) Effect of chain extender and light stabilizer on the weathering resistance of PBAT/PLA blend films prepared by extrusion blowing. Polym Degrad Stab 183:109455. https://doi.org/10.1016/J.POLYMDEGRADSTAB.2020.109455
34. Kijchavengkul T, Auras R, Rubino M et al (2010) Atmospheric and soil degradation of aliphatic-aromatic polyester films. Polym Degrad Stab 95:99–107. https://doi.org/10.1016/j.polymdegradstab.2009.11.048
35. González-López ME, Martín del Campo AS, Robledo-Ortíz JR et al (2020) Accelerated weathering of poly(lactic acid) and its biocomposites: a review. Polym Degrad Stab 179:109290. https://doi.org/10.1016/J.POLYMDEGRADSTAB.2020.109290
36. Lucas N, Bienaime C, Belloy C et al (2008) Polymer biodegradation: Mechanisms and estimation techniques—a review. Chemosphere 73:429–442
37. Ceci-Ginistrelli E, Pugliese D, Boetti NG et al (2016) Novel biocompatible and resorbable UV-transparent phosphate glass based optical fiber. Opt Mater Express 6:2040. https://doi.org/10.1364/ome.6.002040
38. Sciancalepore C, Togliatti E, Giubilini A et al (2022) Preparation and characterization of innovative poly(butylene adipate terephthalate)-based biocomposites for agri-food packaging application. J Appl Polym Sci. https://doi.org/10.1002/app.52370
39. Felix de Andrade M, de Lima D, Silva I, Alves da Silva G et al (2020) A study of poly (butylene adipate-co-terephthalate)/orange essential oil films for application in active antimicrobial packaging. LWT 125:109148. https://doi.org/10.1016/J.LWT.2020.109148
40. Sciancalepore C, Moroni F, Messori M, Bondioli F (2017) Acrylate-based silver nanocomposite by simultaneous

polymerization–reduction approach via 3D stereolithography. Compos Commun 6:11–16. https://doi.org/10.1016/j.coco.2017.07.006
41. Saba N, Jawaid M, Alothman OY, Paridah MT (2016) A review on dynamic mechanical properties of natural fibre reinforced polymer composites. Constr Build Mater 106:149–159. https://doi.org/10.1016/j.conbuildmat.2015.12.075
42. Pothan LA, Oommen Z, Thomas S (2003) Dynamic mechanical analysis of banana fiber reinforced polyester composites. Compos Sci Technol 63:283–293
43. Vlasveld DPN, Bersee HEN, Picken SJ (2005) Creep and physical aging behaviour of PA6 nanocomposites. Polymer (Guildf) 46:12539–12545. https://doi.org/10.1016/j.polymer.2005.10.120
44. Jawaid M, Abdul Khalil HPS, Hassan A et al (2013) Effect of jute fibre loading on tensile and dynamic mechanical properties of oil palm epoxy composites. Compos B Eng 45:619–624. https://doi.org/10.1016/j.compositesb.2012.04.068
45. Wang J-S, Porter RS (1995) On the viscosity-temperature behavior of polymer melts. Rheol Acta 34:496–503. https://doi.org/10.1007/BF00396562
46. Sciancalepore C, Bondioli F, Messori M (2017) Non-hydrolytic sol–gel synthesis and reactive suspension method: an innovative approach to obtain magnetite–epoxy nanocomposite materials. J Sol-Gel Sci Technol 81:69–83. https://doi.org/10.1007/s10971-016-4095-z
47. Kang S, Hong S II, Choe CR et al (2001) Preparation and characterization of epoxy composites filled with functionalized nanosilica particles obtained via sol-gel process. Polymer (Guildf) 42:879–887
48. Romanzini D, Lavoratti A, Ornaghi HL et al (2013) Influence of fiber content on the mechanical and dynamic mechanical properties of glass/ramie polymer composites. Mater Des 47:9–15. https://doi.org/10.1016/J.MATDES.2012.12.029
49. Phothisarattana D, Wongphan P, Promhuad K et al (2022) Blown film extrusion of PBAT/TPS/ZnO nanocomposites for shelf-life extension of meat packaging. Colloids Surf B 214:112472. https://doi.org/10.1016/J.COLSURFB.2022.112472
50. Dorigato A, D'Amato M, Pegoretti A (2012) Thermo-mechanical properties of high density polyethylene—Fumed silica nanocomposites: effect of filler surface area and treatment. J Polym Res. https://doi.org/10.1007/s10965-012-9889-2
51. Togliatti E, Laporta CC, Grimaldi M et al (2021) Preparation and characterisation of PBAT-based biocomposite materials reinforced by protein complex microparticles. Mater Proc 7:20. https://doi.org/10.3390/IOCPS2021-12019
52. Militký J, Jabbar A (2015) Comparative evaluation of fiber treatments on the creep behavior of jute/green epoxy composites. Compos B Eng 80:361–368. https://doi.org/10.1016/J.COMPOSITESB.2015.06.014
53. Durante M, Formisano A, Boccarusso L et al (2017) Creep behaviour of polylactic acid reinforced by woven hemp fabric. Compos B Eng 124:16–22. https://doi.org/10.1016/J.COMPOSITESB.2017.05.038
54. Yang J-L, Zhang Z, Schlarb AK, Friedrich K (2006) On the characterization of tensile creep resistance of polyamide 66 nanocomposites. Part I. Experimental results and general discussions. Polymer. https://doi.org/10.1016/j.polymer.2006.02.065
55. Feldman D (2002) Polymer weathering: photo-oxidation. J Polym Environ 10:163–173. https://doi.org/10.1023/A:1021148205366
56. Kockott D (1989) Natural and artificial weathering of polymers. Polym Degrad Stab 25:181–208. https://doi.org/10.1016/S0141-3910(89)81007-9
57. Cai Y, Lv J, Feng J (2013) Spectral characterization of four kinds of biodegradable plastics: poly (lactic acid), poly (butylenes adipate-co-terephthalate), poly (hydroxybutyrate-co-hydroxyvalerate) and poly (butylenes succinate) with FTIR and Raman spectroscopy. J Polym Environ 21:108–114. https://doi.org/10.1007/s10924-012-0534-2
58. Shankar S, Rhim JW (2016) Tocopherol-mediated synthesis of silver nanoparticles and preparation of antimicrobial PBAT/silver nanoparticles composite films. LWT Food Sci Technol 72:149–156. https://doi.org/10.1016/j.lwt.2016.04.054
59. Bumbudsanpharoke N, Wongphan P, Promhuad K et al (2022) Morphology and permeability of bio-based poly(butylene adipate-co-terephthalate) (PBAT), poly(butylene succinate) (PBS) and linear low-density polyethylene (LLDPE) blend films control shelf-life of packaged bread. Food Control 132:108541. https://doi.org/10.1016/J.FOODCONT.2021.108541
60. Scarfato P, Acierno D, Russo P (2015) Photooxidative weathering of biodegradable nanocomposite films containing halloysite. Polym Compos 36:1169–1175. https://doi.org/10.1002/pc.23478
61. Silverstein RM, Webster FX, Kiemle DJ (2005) Spectrometric identification of organic compounds, 7th edn. Wiley, Hoboken, NJ
62. Doğan F, Şirin K, Kolcu F, Kaya İ (2018) Conducting polymer composites based on LDPE doped with poly(aminonaphthol sulfonic acid). J Electrostat 94:85–93. https://doi.org/10.1016/j.elstat.2018.07.004
63. Gardette M, Perthue A, Gardette JL et al (2013) Photo- and thermal-oxidation of polyethylene: comparison of mechanisms and influence of unsaturation content. Polym Degrad Stab 98:2383–2390. https://doi.org/10.1016/j.polymdegradstab.2013.07.017
64. Gulmine JV, Janissek PR, Heise HM, Akcelrud L (2002) Polyethylene characterization by FTIR. Polym Test 21:557–563. https://doi.org/10.1016/S0142-9418(01)00124-6
65. Pinheiro IF, Ferreira FV, Alves GF et al (2019) Biodegradable PBAT-based nanocomposites reinforced with functionalized cellulose nanocrystals from *Pseudobombax munguba*: rheological, thermal, mechanical and biodegradability properties. J Polym Environ 27:757–766. https://doi.org/10.1007/s10924-019-01389-z
66. Shah AA, Hasan F, Hameed A, Ahmed S (2008) Biological degradation of plastics: a comprehensive review. Biotechnol Adv 26:246–265
67. Wongphan P, Panrong T, Harnkarnsujarit N (2022) Effect of different modified starches on physical, morphological, thermomechanical, barrier and biodegradation properties of cassava starch and polybutylene adipate terephthalate blend film. Food Packag Shelf Life 32:100844. https://doi.org/10.1016/J.FPSL.2022.100844
68. Döhler F, Mandlule A, van Wüllen L et al (2015) 31 P NMR characterisation of phosphate fragments during dissolution of calcium sodium phosphate glasses. J Mater Chem B 3:1125–1134. https://doi.org/10.1039/C4TB01757A
69. Mikhailenko NY, Stroganova EE, Buchilin NV (2013) Solubility of calcium phosphate glasses and glass ceramic materials in water and physiological media. Glass Ceram (English translation of Steklo i Keramika) 70:158–163. https://doi.org/10.1007/S10717-013-9531-8/FIGURES/4
70. Iggui K, le Moigne N, Kaci M et al (2015) A biodegradation study of poly(3-hydroxybutyrate-co-3-hydroxyvalerate)/organoclay nanocomposites in various environmental conditions. Polym Degrad Stab 119:77–86. https://doi.org/10.1016/j.polymdegradstab.2015.05.002

Publisher's Note Springer Nature remains neutral with regard to jurisdictional claims in published maps and institutional affiliations.